

Prospects for gravitational-wave detection and supermassive black hole astrophysics with pulsar timing arrays

V. Ravi^{1,2*}, J. S. B. Wyithe¹, R. M. Shannon² and G. Hobbs²

¹*School of Physics, University of Melbourne, Parkville VIC 3010, Australia*

²*CSIRO Astronomy and Space Science, Australia Telescope National Facility, P.O. Box 76, Epping, NSW 1710, Australia*

ABSTRACT

Large-area sky surveys show that massive galaxies undergo at least one major merger in a Hubble time. Ongoing pulsar timing array (PTA) experiments are aimed at measuring the gravitational wave (GW) emission from binary supermassive black holes (SMBHs) at the centres of galaxy merger remnants. In this paper, using the latest observational estimates for a range of galaxy properties and scaling relations, we predict the amplitude of the GW background generated by the binary SMBH population. We also predict the numbers of individual binary SMBH GW sources. We predict the characteristic strain amplitude of the GW background to lie in the range $5.1 \times 10^{-16} < A_{\text{yr}} < 2.4 \times 10^{-15}$ at a frequency of $(1 \text{ yr})^{-1}$, with 95% confidence. Higher values within this range, which correspond to the more commonly preferred choice of galaxy merger timescale, will fall within the expected sensitivity ranges of existing PTA projects in the next few years. In contrast, we find that a PTA consisting of at least 100 pulsars observed with next-generation radio telescopes will be required to detect continuous-wave GWs from binary SMBHs. We further suggest that GW memory bursts from coalescing SMBH pairs are not viable sources for PTAs. Both the GW background and individual GW source counts are dominated by binaries formed in mergers between early-type galaxies of masses $\gtrsim 5 \times 10^{10} M_{\odot}$ at redshifts $\lesssim 1.5$. Uncertainties in the galaxy merger timescale and the SMBH mass – galaxy bulge mass relation dominate the uncertainty in our predictions.

Key words: black hole physics — galaxies: evolution — gravitational waves — pulsars: general

1 INTRODUCTION

Astrophysical gravitational waves (GWs) affect long-term timing measurements of radio pulsars (Estabrook & Wahlquist 1975; Sazhin 1978; Detweiler 1979). GW-induced metric perturbations at the Earth cause variations in pulse arrival times that differ between pulsars only by geometric factors. Hence, a specific GW signal may be directly detected in contemporaneous timing measurements of multiple pulsars. Three such ‘pulsar timing arrays’ (PTAs; e.g., Foster & Backer 1990)

are currently in operation: the European Pulsar Timing Array (EPTA; Kramer & Champion 2013), the North American Nanohertz Observatory for Gravitational Waves (NANOGrav; McLaughlin 2013), and the Parkes Pulsar Timing Array (PPTA; Manchester et al. 2013). These groups also share data as part of the International Pulsar Timing Array (IPTA; Hobbs et al. 2010) consortium. Currently, at least 50 millisecond pulsars are observed every 2 – 4 weeks, and data sets stretching for 5 – 30 yr exist for 34 of these pulsars (Manchester & IPTA 2013). Together, these timescales imply that PTAs are sensitive to GWs in the frequency band $10^{-9} - 10^{-7}$ Hz, which is complementary to other GW detection experiments.

* E-mail: v.vikram.ravi@gmail.com

The best-studied sources of GWs within the PTA frequency band are binary supermassive black holes (SMBHs). Stellar- or gas-dynamical evidence exists for SMBHs at the centres of 87 nearby galaxies at the time of writing (Kormendy & Ho 2013), with masses M_\bullet ranging between $10^6 - 10^{11} M_\odot$. Phenomenological models of the buildup of the cosmological mass density in SMBHs during luminous quasar phases for redshifts $z < 5$ (e.g., Yu & Tremaine 2002; Shankar et al. 2013) suggest short quasar lifetimes. This, considered together with local correlations between M_\bullet and, for example, galaxy bulge mass M_{bul} (e.g., Kormendy & Ho 2013), suggests that all massive galaxies ($M_* > 10^{10} M_\odot$) which formed since the $z \sim 2$ peak of quasar activity host SMBHs (see also Miller et al. 2014).

In the context of hierarchical structure formation, mergers are integral to the formation histories of massive galaxies, and evidence for interacting galaxies is seen across most of cosmic time (Barnes & Hernquist 1992). Multiple SMBHs are expected to be found in galaxy merger products. Indeed, pairs of active galactic nuclei (AGN) are observed in galaxies in the late stages of mergers (Merritt & Milosavljević 2005), with projected separations as small as 7 pc (Rodriguez et al. 2006). The central SMBHs in a pair of merging galaxies are likely to sink in the merger remnant potential well through dynamical friction and form a bound binary (e.g., Begelman et al. 1980; Khan et al. 2012). Dynamical friction becomes inefficient once stars within the binary orbit are ejected, and the slingshot scattering of stars on radial orbits (Frank & Rees 1976; Quinlan 1996; Yu 2002) or friction against circumbinary gas (Escala et al. 2004; Dotti et al. 2007; Roedig et al. 2011) is required to drive further orbital decay. At a binary component separation of $\ll 1$ pc, energy and angular momentum losses to gravitational wave (GW) emission can lead to SMBH-SMBH coalescence within a Hubble time (e.g., Peters & Mathews 1963). A few candidate binary SMBHs with such separations have been identified (e.g., Valtonen et al. 2008; Boroson & Lauer 2009; Eracleous et al. 2012).

The existence of a large cosmological population of binary SMBHs is thus inferred, some of which emit GWs in the PTA frequency band. If the orbits of all binary SMBHs radiating GWs in the PTA frequency band are circular and evolving under GW emission alone, the summed GW signals from all binaries together have the expected spectral form (e.g., Phinney 2001):

$$h_c(f) = A_{\text{yr}} \left(\frac{f}{f_{\text{yr}}} \right)^{-2/3}. \quad (1)$$

Here, $h_c(f)$ is the GW characteristic strain per logarithmic frequency unit, f is the GW frequency at the Earth, $f_{\text{yr}} = (1 \text{ yr})^{-1}$ and A_{yr} is the characteristic spectral amplitude at f_{yr} . The summed signals from binary SMBHs may be collectively modelled as a GW background (GWB). GWs from individual binaries may be detectable as continuous-wave (CW) sources (e.g., Sesana et al. 2009; Ravi et al. 2012). Coalescing pairs of SMBHs also emit GW ‘memory’ bursts (Braginskii & Thorne 1987; Favata 2009), which are

abrupt, propagating metric changes that also affect pulsar timing measurements (e.g., Madison et al. 2014).

Of these three types of GW signal, searches for a GWB provide the best constraints on models for the binary SMBH population (Shannon et al. 2013) and are perhaps the closest to yielding a successful detection (Siemens et al. 2013). Shannon et al. (2013) used the first PPTA data release (Manchester et al. 2013) to show that $A_{\text{yr}} < 2.4 \times 10^{-15}$ with 95% confidence. Siemens et al. (2013) suggest that the NANOGrav PTA is likely to be able to detect a GWB with $A_{\text{yr}} = 10^{-15}$ by around the year 2020. Constraints on GWs from individual binary SMBHs with the current PPTA data set showed that binaries with component masses $M_\bullet > 10^9 M_\odot$ and with separations of less than 0.02 pc are unlikely to exist within 30 Mpc of the Earth (Zhu et al. 2014). No search for memory bursts with PTA data has so far been published. Wang et al. (submitted) describe an unsuccessful search for memory bursts using current PPTA data.

Predictions for GW signals from binary SMBHs are based either on physical models for galaxy formation and evolution which predict the binary SMBH population, or on directly observed quantities such as the galaxy merger rate and SMBH-galaxy scaling relations. The former predictions typically combine dark matter halo merger rates in the cold dark matter paradigm, analytic or numerical estimates of galaxy merger and binary SMBH formation timescales, prescriptions for the cosmic evolution of the galaxy and SMBH population and the assumption of GW-driven binary orbital evolution (Wyithe & Loeb 2003; Enoki et al. 2004; Sesana et al. 2008; Ravi et al. 2012; Kulier et al. 2013; Ravi et al. 2014). Once tuned to reproduce observables such as local SMBH-galaxy relations, the galaxy stellar mass function (GSMF) and colour distribution, and the quasar luminosity function, these models result in estimates of A_{yr} in the range $10^{-16} - 2 \times 10^{-15}$. The exact value depends on, for example, the assumed cosmological parameters, galaxy merger timescales and the specific models for SMBH formation and growth. Models for the binary SMBH population which more directly incorporate observational information (Jaffe & Backer 2003; Sesana 2013; McWilliams et al. 2014) result in similar values of A_{yr} . While various studies suggest that individual binary SMBHs may be viable CW sources of GWs for PTAs (Sesana et al. 2009; Ravi et al. 2012) as well as viable sources of memory bursts (van Haasteren & Levin 2010; Cordes & Jenet 2012; Madison et al. 2014), quantitative predictions of source counts have only been calculated for CW sources using theoretical galaxy formation models (Sesana et al. 2009).

In this paper, we adopt an observations-based approach towards modelling the binary SMBH population, in order to predict the range of GW signals in the PTA frequency band. A similar study by Sesana (2013), hereafter S13, combined a plethora of observational estimates of the merger rate of massive galaxies, the GSMF and local SMBH-galaxy relations to derive a range of possible GWB amplitudes. However, some of the observational quantities included in the S13 study do not represent the best current knowledge. Fur-

thermore, some relevant uncertainties, such as in the possible redshift evolution of the SMBH-galaxy relations, were not accounted for by S13, and no predictions for individual GW sources were made. Besides addressing these issues, this paper builds on previous studies in the following ways:

- We quantify the impacts of different observational uncertainties on the amplitude of the GWB generated by binary SMBHs. We focus in particular on aspects of our model for the binary SMBH population for which little observational information currently exists.
- We highlight the redshifts, masses and types of merging galaxies which result in binary SMBHs which dominate the GWB amplitude.
- We provide new, observations-based predictions for the counts of individual GW sources. We further present the first estimates for the expected numbers of detectable individual GW sources, given different PTA configurations, that are robust with respect to pulsar parameter fitting.

In §2, we outline our model, and present our results in §3. We state the key implications of this work for PTAs in §4. Finally, we discuss these results in §5, and summarise our conclusions in §6. Throughout this work, we adopt a concordance cosmology based on results from the *Planck* satellite (Planck Collaboration et al. 2013), including $H_0 = 67.8 \text{ km s}^{-1} \text{ Mpc}^{-1}$, $\Omega_\Lambda = 0.692$ and $\Omega_M = 0.308$.

2 AN EMPIRICAL MODEL FOR GWS FROM BINARY SMBHS

2.1 The SMBH-SMBH coalescence rate

The cosmological population of binary SMBHs emitting GWs in the PTA frequency band can be characterised using the SMBH-SMBH coalescence rate. The numbers of binary SMBHs in different orbits are related to the coalescence rate through a continuity equation (Phinney 2001; Ravi et al. 2014) that includes assumptions about the rate of binary SMBH orbital evolution.

We assume that the SMBH-SMBH coalescence rate is equivalent to the galaxy merger rate. This is justified because massive galaxy mergers are typically completed within a few galaxy dynamical times, whereas the timescales for two SMBHs to form a gravitationally-bound binary and then coalesce through losses of energy and angular momentum to their environments and GWs are much shorter (e.g., Begelman et al. 1980; Roedig & Sesana 2012). In this work, we neglect systems of more than two gravitationally-interacting SMBHs resulting from multiple galaxy mergers, because we expect these to be rare for the high mass ratio ($\mu_* > 1/3$) mergers between massive ($M_* > 10^{10} M_\odot$) galaxies that we consider. We further assume that each galaxy contains a central SMBH with a mass related to the galaxy bulge mass. We use measured quantities to determine the all-sky coalescence rate of pairs of SMBHs. For each quantity, we define a fiducial prescription, and also describe the possible ranges over which the prescription can vary.

Similarly to S13, we express the galaxy merger rate as

$$\Phi_{\text{mrg}}(M_*, \mu_*, z) = \frac{d^4 N_{\text{mrg}}}{d \log(M_*) d \log(\mu_*) dz dt} \quad (2)$$

$$= \frac{1}{\Gamma} \frac{dt_p}{dt} \frac{d^2 N_{\text{gal}}}{d \log(M_*) dz} \frac{dP}{d \log(\mu_*)} \Big|_{M_*} \quad (3)$$

where N_{mrg} is the number of mergers between two galaxies of combined stellar mass $M_*(1 + \mu_*)$, μ_* is the ratio between the smaller and larger galaxy stellar masses and z is the cosmological redshift. The merger rate, Φ_{mrg} , is defined as the number of mergers per units M_* , μ_* , z and observer time t . In Equation 3, N_{gal} is the number of galaxies across the entire sky with a given M_* at a given z . This is related to the standard GSMF, $\Phi_*(M_*, z)$, as

$$\frac{d^2 N_{\text{gal}}}{d \log(M_*) dz} = \Phi_* \frac{4\pi d^2 V_c}{d \Omega dz}, \quad (4)$$

where $\frac{4\pi d^2 V_c}{d \Omega dz}$ is the sky-integrated comoving volume shell between redshifts z and $z + dz$. In Equation 4, $\frac{dP}{d \log(\mu_*)} \Big|_{M_*}$ is the probability density function for a galaxy merger event with mass M_* at redshift z having a mass ratio μ_* , $\Gamma(M_*, z) = \left(\frac{dn_{\text{mrg}}}{dt_p} \right)^{-1}$ is the average proper time between major mergers for a galaxy with a mass M_* at redshift z and $\frac{dt_p}{dt} = (1+z)^{-1}$. Also, $\frac{dn_{\text{mrg}}}{dt_p} \Big|_{M_*, z}$ is the number of mergers, n_{mrg} , per unit proper time, t_p , for a single galaxy with a mass M_* at redshift z .

In order to convert galaxy stellar masses to bulge masses (M_{bul}) we distinguish between quiescent, red-sequence early-type galaxies and star-forming, blue-cloud late-type galaxies. We write the total GSMF as a sum of the GSMFs of early- ($\Phi_{*, \text{early}}$) and late-type ($\Phi_{*, \text{late}}$) galaxies:

$$\Phi_*(M_*, z) = \Phi_{*, \text{early}} + \Phi_{*, \text{late}}. \quad (5)$$

We relate M_* to M_{bul} for early- and late-type galaxies using a scheme described in §2.1.3.

To convert between M_{bul} and the central SMBH masses (M_\bullet) we use the widely-known $M_\bullet - M_{\text{bul}}$ relation (Kormendy & Ho 2013; Scott et al. 2013). In contrast to S13, we express this relation as

$$\frac{dP}{d \log M_\bullet} = \mathcal{N}(\alpha + \beta \log M_{\text{bul}}, \epsilon^2) \quad (6)$$

where $\mathcal{N}(\mu, \sigma^2)$ denotes a normal probability density function with centre μ and variance σ^2 and α , β and the intrinsic scatter, ϵ , are observationally-determined constants. It is important to account for intrinsic scatter in the $M_\bullet - M_{\text{bul}}$ relation when inferring the SMBH mass function from the bulge mass function (e.g., Aller & Richstone 2002), because to not do so would lead to the SMBH mass function being underestimated.

2.1.1 The times between galaxy mergers

Observational estimates of $\Gamma(M_*, z)$ require knowledge of the fraction of galaxies, f_{gm} , within a mass-complete sample at a given redshift that are undergoing mergers, and the

proper time τ_m during which merger events can be observationally identified (for a review, see Conselice 2014). Then, $\Gamma(M_*, z) = \tau_m / f_{\text{gm}}$. In this work, we focus on major mergers with stellar mass ratios $\mu_* \geq 1/3$, because these systems are likely to dominate the GW signal (e.g., Sesana et al. 2004, S13).

We consider three recent measurements of f_{gm} for major mergers at different redshifts in wide-area galaxy surveys, which are largely complete for galaxy stellar masses $M_* > 10^{10} M_\odot$. These three studies fit their data to the function $f_{\text{gm}} = a_{\text{gm}}(1+z)^{b_{\text{gm}}}$, where a_{gm} and b_{gm} are free parameters.

- Conselice et al. (2009) used structural analyses of concentration, asymmetry and clumpiness (the ‘CAS’ parameters) to identify systems in the process of merging among ~ 22000 galaxies in the COSMOS and Extended Groth Strip surveys with $M_* > 10^{10} M_\odot$ at $z < 1.2$. This technique is sensitive to major mergers in particular, with mass ratios $\mu_* \gtrsim 1/3$ (Conselice 2003). Conselice et al. (2009) found $f_{\text{gm}} = (0.022 \pm 0.006)(1+z)^{1.6 \pm 0.6}$.

- Xu et al. (2012) counted galaxy pairs with projected separations between $5 \text{ h}^{-1} \text{ kpc}$ and $20 \text{ h}^{-1} \text{ kpc}$ from the COSMOS survey to estimate f_{gm} for $z < 1$ and $\mu_* > 0.4$. They scaled their results to include galaxy pairs for all $\mu_* \geq 1/3$ using the argument that f_{gm} is inversely proportional to the logarithm of minimum mass ratio of the observed galaxy pair sample. Xu et al. (2012) found $f_{\text{gm}} = (0.013 \pm 0.001)(1+z)^{2.2 \pm 0.2}$.

- Both the above works may suffer from incorporating small galaxy samples at low redshifts. This issue was addressed by Robotham et al. (2014) using a large sample of galaxy pairs from the Galaxy and Mass Assembly (GAMA) survey in the redshift interval $0.05 < z < 0.2$. When standardised to the same projected separation, galaxy mass and mass ratio windows as Xu et al. (2012), they found a substantially higher value of f_{gm} at these redshifts. By combining their results with all recent measurements of f_{gm} at redshifts up to 1.2, and normalising to the same projected pair separations of Xu et al. (2012), Robotham et al. (2014) found $f_{\text{gm}} = (0.021 \pm 0.001)(1+z)^{1.53 \pm 0.08}$.

Other works have estimated f_{gm} with varying levels of accuracy. S13 included results from the galaxy pair studies of Bundy et al. (2009), de Ravel et al. (2009) and López-Sanjuan et al. (2012). However, Bundy et al. (2009) and de Ravel et al. (2009) had significantly smaller pair samples than were utilised by either Xu et al. (2012) or Robotham et al. (2014), and López-Sanjuan et al. (2012) only considered major mergers of galaxies with $M_* > 10^{11} M_\odot$.

In the absence of observational estimates of the galaxy merger timescale (τ_m) used in calculating $\Gamma(M_*, z)$ from different measurements of f_{gm} , we make use of theoretical predictions. However, the range of possible predictions spans a factor of three. Kitzbichler & White (2008) used a mock galaxy catalogue from a semi-analytic model implemented within the Millennium simulation (Springel et al. 2005) to estimate τ_m for galaxies with different masses at different stages of merging assuming circular galaxy

orbits and angular momentum loss through dynamical friction. However, a suite of hydrodynamic simulations of galaxy mergers conducted by Lotz et al. (2008) and Lotz et al. (2010), hereafter collectively L08, resulted in significantly shorter merger timescales. While some authors (e.g., Bundy et al. 2009; Robotham et al. 2014) use the estimates of Kitzbichler & White (2008) to calculate $\Gamma(M_*, z)$, others (e.g., Conselice et al. 2009; Xu et al. 2012; Conselice 2014) argue that these estimates are incorrect, at least for major mergers (see footnote 15 of Hopkins et al. 2010). Analyses of cosmological hydrodynamical simulations combining dark matter and baryonic components suggest that the merger timescales assumed in semi-analytic models of galaxy formation and used by Kitzbichler & White (2008) are overestimated for major mergers (Jiang et al. 2008). Furthermore, L08 presented estimates of τ_m specifically calibrated to the CAS technique of Conselice et al. (2009) using mock galaxy images. Here, as a fiducial case, we only use the estimates of τ_m from L08, specific to estimates of f_{gm} from both galaxy pair counts and CAS analyses. These merger timescales were averaged over both field and cluster environments, and hence account for environmental dependencies. However, the simulation suite of L08 was not large enough to reveal significant mass- or redshift-dependence of τ_m . Hence, we consider it possible that the weak dependencies on these quantities identified by Kitzbichler & White (2008) may be present.

We therefore have the three following estimates of the times between galaxy mergers:

$$\Gamma(M_*, z) = (13.8 \pm 3.1)(1+z)^{-1.6 \pm 0.6} \text{ Gyr} \quad (7)$$

$$\Gamma(M_*, z) = (19.2 \pm 1.5)(1+z)^{-2.2 \pm 0.2} \text{ Gyr} \quad (8)$$

$$\Gamma(M_*, z) = (14.3 \pm 0.6)(1+z)^{-1.6 \pm 0.6} \text{ Gyr}, \quad (9)$$

based on the work of Conselice et al. (2009), Xu et al. (2012) and Robotham et al. (2014) respectively. While we consider each of Equations 7–9 to be equally possible, we choose Equation 7 (Conselice et al. 2009) as a fiducial prescription. The possible mass- and redshift-dependence of $\Gamma(M_*, z)$ is given by the factor $(M_*/10^{10.7} M_\odot)^{-0.3}(1+z/8)$ (Kitzbichler & White 2008); we further consider it equally likely that this factor is present or absent, while choosing its absence as fiducial. Together, there are then six different possibilities for $\Gamma(M_*, z)$ that we consider, each with observational uncertainties. We also demonstrate the effects on the GW signal from binary SMBHs of using systematically larger values of τ_m that are consistent with Kitzbichler & White (2008).

The fitting formulae in Equations 7–9 are consistent with results at higher redshifts (Conselice 2014). We hence adopt these equations for $z < 3$, and also assume $\frac{dP}{d \log(\mu_*)} = \text{constant}$ (Xu et al. 2012). Uncertainties in $\Gamma(M_*, z)$ for $z \gtrsim 1$ do not significantly affect our predictions for GW signals from binary SMBHs, because, as we demonstrate, it appears that these signals are dominated by contributions from binary SMBHs at lower redshifts.

2.1.2 The GSMF

We use the latest measurements of the GSMF for $z < 3$ in the range $10^{10} M_{\odot} \leq M_{*} \leq 10^{12} M_{\odot}$ based on the COSMOS/UltraVISTA catalogue (Muzzin et al. 2013). Muzzin et al. (2013) present GSMFs for quiescent (early-type) and star-forming (late-type) galaxies, which were identified using a colour cut. Utilising UV to mid-IR galaxy photometry, with improved sensitivity and sky-coverage over previous compilations, these authors provide the most accurate determinations of the early- and late-type GSMFs currently available.

However, we still need to account for a selection of systematic errors. Muzzin et al. (2013) use redshift, luminosity and mass measurements obtained through spectral energy distribution analyses. Assuming galaxy magnitude measurements of sufficient accuracy, systematic errors in the photometric redshifts and galaxy stellar mass measurements are dominated by how the stellar populations are modelled (e.g., Bernardi et al. 2010; Mitchell et al. 2013; Courteau et al. 2014). Systematic errors in stellar mass measurements can lead to errors in the GSMF of greater than 0.6 dex (Mitchell et al. 2013). Muzzin et al. (2013) present five separate determinations of the GSMFs of early- and late-type galaxies using different choices for the stellar population synthesis model and star formation history, as well as expanded possibilities for galaxy metallicities and dust attenuation laws. We assume that each of these five GSMF determinations, for which Schechter function fits are given in Table 3 of Muzzin et al. (2013), are equally likely to be correct, but choose the default GSMF of Muzzin et al. (2013), given in their Table 1, as fiducial.

The method of colour selection used to identify early- and late-type galaxies adds further systematic uncertainty to the GSMF estimates. For example, Bernardi et al. (2010) showed that edge-on dusty spiral galaxies are in fact the reddest among the galaxy population, and that more than a third of a red-sequence sample of galaxies could be actively star-forming objects. While Bernardi et al. (2010) suggest further simple morphological selections based on galaxy light concentrations to mitigate these effects, these data were not available in the COSMOS/UltraVISTA catalogue. Instead, we use a crude estimation of the uncertainty range of the GSMF caused by the colour selection from Muzzin et al. (2013), who presented GSMFs determined for significantly different colour cuts to their fiducial scheme (their Table 4). We consider this entire range of variability in the GSMF to be possible. We also demonstrate the effects on the resulting GW signal of possible contamination of colour-selected early-type galaxy samples with late-type galaxies in an extreme scenario by also performing our calculations with the early-type GSMF reduced by 1/3.

2.1.3 Relating M_{*} to M_{bul}

The scheme we use to relate M_{*} to M_{bul} for different types of galaxies is summarised as follows.

- Of late-type galaxies with $M_{*} > 10^{10} M_{\odot}$, less than

10% have no bulge component (Mendel et al. 2014); in this work, we assume a conservative value of 10%. Of the others, M_{bul}/M_{*} is in the range 0.2 ± 0.1 (Lackner & Gunn 2012; Mendel et al. 2014; Meert et al. 2014).

- Early-type galaxies with $M_{*} > 10^{10} M_{\odot}$ consist of a significant fraction that are best modelled with both bulges and disks, which are identified with the S0 (lenticular) galaxy population (Lackner & Gunn 2012; Mendel et al. 2014; Meert et al. 2014). These galaxies have values of M_{bul}/M_{*} which are approximately log-normally distributed with mean 0.7 and log-deviation 0.07 dex. A mild correlation between M_{bul}/M_{*} and M_{*} may be present for S0 galaxies (Mendel et al. 2014), which we neglect in this work.

- For $10^{10} M_{\odot} < M_{*} \lesssim 10^{11.25} M_{\odot}$, approximately 75% of early-type galaxies are S0s and 25% are true ellipticals (Emsellem et al. 2011). These fractions change to 55% and 45% respectively for larger stellar masses.

While these results are quite approximate, and only derived for a low-redshift ($z \lesssim 0.3$) galaxy sample, we adopt them as a fiducial scheme for relating M_{*} to M_{bul} for $z < 3$. This scheme is roughly consistent with that used by S13.

In the same way as accounting for scatter in the $M_{\bullet} - M_{\text{bul}}$ relation raises the inferred SMBH mass function (e.g., Aller & Richstone 2002), the bulge mass function inferred from the GSMF will be raised given scatter in relating M_{*} to M_{bul} . Scatter in the $M_{\text{bul}} - M_{*}$ relations can be simply combined with the scatter in the $M_{\bullet} - M_{\text{bul}}$ relation by modifying Equation 6 as follows:

$$\frac{dP}{d \log M_{\bullet}} = \mathcal{N} [\log \alpha + \beta \log(M_{\text{bul}}(M_{*})), \epsilon^2 + \beta^2 \sigma_{\text{bul}}^2], \quad (10)$$

where we assume $\sigma_{\text{bul}} = 0.1$ for both early- and late-type galaxies. In summary, the function $M_{\text{bul}}(M_{*})$ in our fiducial model is defined by

$$M_{\text{bul}}(M_{*}) = \begin{cases} 0.2M_{*}, & \text{for 90\% of late types,} \\ 0.7M_{*}, & \text{for S0s} \\ M_{*}, & \text{for ellipticals} \end{cases} \quad (11)$$

We demonstrate the effects of possible errors in the fraction of early-type galaxies which are ellipticals by considering cases where this fraction is reduced and increased by 50%.

2.1.4 Relating M_{bul} to M_{\bullet}

Despite intense interest in evincing the $M_{\bullet} - M_{\text{bul}}$ relation over the last 15 years, the form of the relation remains uncertain (Kormendy & Ho 2013; Scott et al. 2013). Kormendy & Ho (2013) argue that the $M_{\bullet} - M_{\text{bul}}$ relation is well modelled by a single power law for all galaxies containing classical bulges which include ellipticals, S0s and spirals with bulges displaying steep central light gradients. However, Scott et al. (2013) find, using an extended version of the galaxy sample of Graham et al. (2011) and independent measurements of M_{bul} , that two power laws are required, with a break at $M_{\text{bul}} = 3 \times 10^{10} M_{\odot}$. A physical distinction between the two power laws was identified by splitting

the sample into ‘cusp’ galaxies with steep power-law central light gradients and galaxies where ‘cores’, or light-deficits with respect to a cusp, are present. Cusp galaxies are typically of lower masses than core galaxies, and were found by Scott et al. (2013) to have a steeper log-linear $M_\bullet - M_{\text{bul}}$ relation than core galaxies.

While we consider the $M_\bullet - M_{\text{bul}}$ relations of Kormendy & Ho (2013) and Scott et al. (2013) equally likely, we choose the simpler relation of Kormendy & Ho (2013) as a fiducial case. In Equation 10, Kormendy & Ho (2013) find $\alpha = -4.07 \pm 0.05$, $\beta = 1.16 \pm 0.08$ and $\epsilon = 0.29$. Scott et al. (2013) instead find $\alpha = -15.37 \pm 0.18$ and $\beta = 2.22 \pm 0.58$ for $M_{\text{bul}} \leq 3 \times 10^{10} M_\odot$ and $\alpha = -1.86 \pm 0.09$ and $\beta = 0.97 \pm 0.14$ for $M_{\text{bul}} > 3 \times 10^{10} M_\odot$. As Scott et al. (2013) do not estimate the intrinsic scatter, we assume $\epsilon = 0.29$ for the entire range of M_{bul} .

We do not consider estimates of the $M_\bullet - M_{\text{bul}}$ relation made substantially prior to Kormendy & Ho (2013) and Scott et al. (2013). Previous estimates are thought to be incorrect because of systematic errors in SMBH and bulge mass estimates, the absence of recently-measured SMBH masses in brightest cluster galaxies, and the presence of galaxies without classical bulges in samples used to fit the relations (for details, see Kormendy & Ho 2013). Various authors infer modest redshift evolution in the $M_\bullet - M_{\text{bul}}$ relation such that the typical ratio M_\bullet/M_{bul} may be up to a factor of ~ 3 larger at $z \gtrsim 2$ than the local value (Kormendy & Ho 2013, and references therein). This can be approximately represented by letting $\alpha = \alpha_0 + \log((1+z)^K)$ with $K = 1$ and α_0 as above. As a fiducial case, however, we assume the conservative value of $K = 0$.

2.2 GW signals from binary and coalescing SMBHs

In this paper, we assume that all binary SMBHs are in circular orbits that evolve only under losses of energy and angular momentum to GWs. While the effects of binary SMBH environments and non-zero orbital eccentricities could modify the GW characteristic strain spectrum from the form in Equation 1 at frequencies up to 10^{-8} Hz at the Earth, these effects are highly uncertain (Ravi et al. 2014, and references therein). For frequencies $f > 10^{-8}$ Hz within the PTA band (e.g., at $f = f_{\text{yr}}$), the characteristic strain spectrum does indeed take the form of Equation (1), because the orbits of all binaries radiating GWs at these frequencies are likely to have circularised because of GW-driven evolution. Our assumption allows for direct comparison with the majority of studies on this topic (Jaffe & Backer 2003; Wyithe & Loeb 2003; Enoki et al. 2004; Sesana et al. 2008; Ravi et al. 2012; Kulier et al. 2013; Sesana 2013), and for the GWB spectrum to be characterised by a single amplitude (A_{yr}).

A circular binary SMBH radiates monochromatic GWs at twice its orbital frequency. We use standard expressions from the literature for the rms GW strain amplitude, h_s (e.g., Equation 7 of Sesana et al. 2008) radiated by a circular binary, and the rms GW-induced sinusoidal variations to the pulse times of arrival (ToAs) from radio pulsars, σ_R

(e.g., Equation 20 of Sesana et al. 2009). Both h_s and σ_R are averaged over all binary orientation parameters. Following Cordes & Jenet (2012), we approximate the strain amplitude of a memory burst from a coalescing binary SMBH as

$$h_{\text{mem}} = 3.3 \times 10^{-16} \left(\frac{\eta_\bullet}{10^8 M_\odot} \right) \left(\frac{1 \text{ Gpc}}{D(z)} \right), \quad (12)$$

where $\eta_\bullet = (M_{\bullet,1} M_{\bullet,2}) / (M_{\bullet,1} + M_{\bullet,2})$ is the reduced mass of the coalescing binary system.

To calculate the GWB amplitude for a population of binary SMBHs, consider a multivariate density function, $f_{\mathbf{X}}$, for the observed binary SMBH coalescence rate, R , in terms of a k -component parameter vector \mathbf{X} with components X_i indexed by an integer i :

$$f_{\mathbf{X}} = \prod_{i=1}^k \frac{\partial[R]}{\partial X_i}. \quad (13)$$

Following, e.g., Sesana et al. (2008), A_{yr} is given by

$$A_{\text{yr}} = \left[f_{\text{yr}} \int \dots \int_{\mathbf{X}} f_{\mathbf{X}} \left(\frac{dt}{df} h_s^2 \right)_{f=f_{\text{yr}}} dX_1 \dots dX_k \right]^{1/2}, \quad (14)$$

Here, $\frac{dt}{df} = \left(\frac{df}{dt} \right)^{-1}$ for the domains of t and f under consideration.

2.3 Assembling the model

Mergers between galaxies containing bulges with masses M_* and $M_*\mu_*$ come in nine types, because the galaxies with each mass may be either elliptical, S0 or late-type. In each case, a different prescription is required to identify the bulge masses of the merging galaxies, and hence the masses of the SMBHs in the merging galaxies. Consider a merger between a galaxy of type i , with mass M_* , and a galaxy of type j , with mass $M_*\mu_*$, where i and j each denote either an elliptical, S0 or late-type galaxy. The fraction of cases where this merger will occur is given by $\frac{\Phi_{*,j}}{\Phi_*}$, where Φ_* is given by Equation 5 and the mass functions are evaluated at a mass $M_*\mu_*$. For early-type galaxies, $\Phi_{*,j}$ is specified according to the fractions of ellipticals and S0s at different masses, and for late-type galaxies, $\Phi_{*,j}$ is simply the fraction which contain bulges. The SMBH masses corresponding to the galaxies of types i and j , $M_{\bullet,i}$ and $M_{\bullet,j}$ respectively, are described by the probability density function in Equation 10 for M_{bul} given by $M_{\text{bul},i}(M_*)$ and $M_{\text{bul},j}(M_*\mu_*)$ respectively. Hence, in order to calculate A_{yr} , we combine Equations 3, 4, 5, 10

and 14 as follows:

$$\begin{aligned}
 \frac{A_{\text{yr}}^2}{f_{\text{yr}}} &= \int_{\log(10^{10} M_{\odot})}^{\log(10^{12} M_{\odot})} d \log M_* \int_0^3 dz \int_{\log(1/3)}^0 d \log \mu_* \\
 &\times \int_{-\infty}^{\infty} d \log M_{\bullet, i} \int_{-\infty}^{\infty} d \log M_{\bullet, j} \\
 &\times \frac{4\pi d^2 V_c}{d\Omega dz} \frac{1}{\Gamma} \frac{dP}{d \log(\mu_*)} \frac{dt_p}{dt} \left(\frac{dt}{df} \right)_{f=f_{\text{yr}}} \\
 &\times \frac{dP}{d \log M_{\bullet, i}} \Big|_{M_*} \frac{dP}{d \log M_{\bullet, j}} \Big|_{M_* \mu_*} \\
 &\times \sum_{i, j} \Phi_{*, i} \frac{\Phi_{*, j}}{\Phi_*} h_s^2(M_{\bullet, i}, M_{\bullet, j}, z, f_{\text{yr}}).
 \end{aligned} \tag{15}$$

We evaluate this integral numerically by summing over the integrand in bins of $\log M_*$, z , $\log \mu_*$, $\log M_{\bullet, i}$, and $\log M_{\bullet, j}$. To determine the predicted numbers of CW sources, we count the numbers of individual binary SMBHs in each bin with different values of h_s radiating GWs at f_{yr} within a nominal bandwidth of $\Delta f = (10 \text{ yr})^{-1}$. We also record the rate of memory bursts in each bin with corresponding amplitudes h_{mem} . These latter operations are equivalent to numerically evaluating the conditional densities of GW sources in terms of h_s and h_{mem} .

Equation 15 builds on the approach of S13 in two ways. First, we account for the effects of intrinsic scatter in the $M_{\bullet} - M_{\text{bul}}$ relation and in relating M_* to M_{bul} . We also attempt to match the numbers of galaxy mergers of different types to the measured GSMFs, rather than assuming the same galaxy pair fractions for all types of mergers.

3 RESULTS

3.1 The GWB amplitude

We first calculated A_{yr} using Equation 15 given the fiducial prescriptions for $\Gamma(M_*, z)$, the GSMF, the scheme relating M_* and M_{bul} and the $M_{\bullet} - M_{\text{bul}}$ relation, as detailed in sections 2.1.1–2.1.4. The resulting fiducial value for A_{yr} was 1.3×10^{-15} . We then identified the possible ranges of A_{yr} consistent with the observational uncertainties in each of $\Gamma(M_*, z)$, the GSMF and the $M_{\bullet} - M_{\text{bul}}$ relation alone. This was accomplished by generating 600 realisations of A_{yr} with the parameters of a single one of these quantities randomised and with the other terms in Equation 15 held fixed at their fiducial values. The process was then repeated with randomisation individually in the other two quantities.

Histograms of the resulting three samples of realisations of A_{yr} are shown in the middle three panels of Figure 1, along with the fiducial value of A_{yr} (as a vertical dashed line). While the possible ranges of A_{yr} given observational uncertainties in $\Gamma(M_*, z)$ and the GSMF are roughly equivalent, observational uncertainty in the $M_{\bullet} - M_{\text{bul}}$ relation results in a slightly larger range of possible A_{yr} values.

We also considered the effects of adopting four modifications to the fiducial model relating to parameters for which current observational constraints are poor. These modifica-

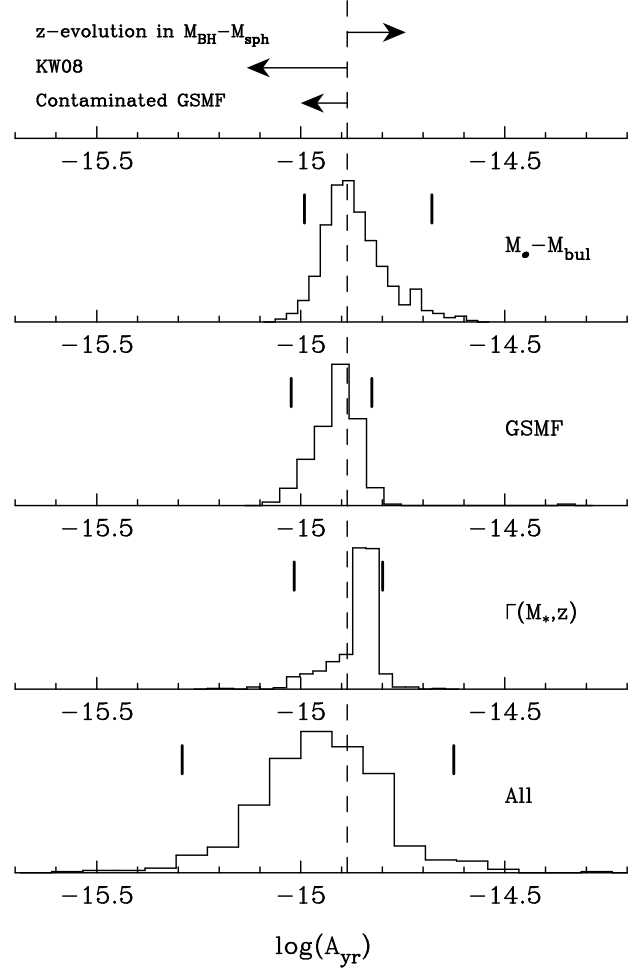


Figure 1. Depiction of uncertainties in the value of A_{yr} calculated using Equation 15. The standardised histograms labelled ‘ $\Gamma(M_*, z)$ ’, ‘GSMF’ and ‘ $M_{\bullet} - M_{\text{bul}}$ ’ show the distributions of 600 realisations of A_{yr} given randomisation over the prescriptions for the respective quantities alone. The vertical dashed line indicates the value of $A_{\text{yr}} = 1.3 \times 10^{-15}$ resulting from the fiducial prescriptions for all quantities in Equation 15. The three arrows at the top of the Figure show how much this fiducial value varies given possible systematic uncertainties in our model. From the bottom, the arrowheads indicate the values of A_{yr} corresponding to a possibly contaminated early-type GSMF, galaxy merger timescales consistent with Kitzbichler & White (2008) and redshift-evolution in the normalisation of the $M_{\bullet} - M_{\text{bul}}$ relation respectively (see text for details). The standardised histogram labelled ‘All’ shows the distribution of 600 realisations of A_{yr} given randomisations over all uncertainties considered in this paper. For all four histograms, the 2.5% and 97.5% percentiles are shown as thick vertical bars.

tions, which were introduced in Subsections 2.1.1–2.1.4, result in the following values of A_{yr} :

- (i) When we decrease the early-type GSMF by a factor of 1/3 to simulate an extreme case of contamination of colour-selected early-type galaxy samples by late-type galaxies (e.g., edge-on spirals), we obtain $A_{\text{yr}} = 10^{-15}$. This represents a decrease of 0.12 dex over the fiducial model.

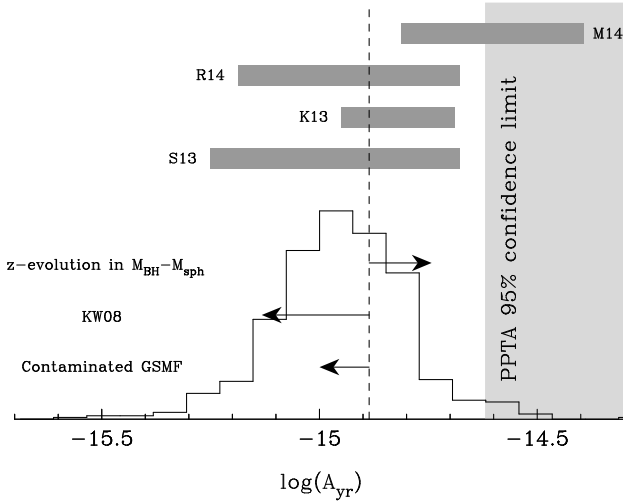


Figure 2. Comparison between our predictions for A_{yr} and those from other works. The histogram is identical to that labelled ‘All’ in Figure 1. The vertical dashed line indicates our fiducial prediction of $A_{\text{yr}} = 1.3 \times 10^{-15}$, and the arrows indicate systematic uncertainties in A_{yr} (see the caption of Figure 1 for details). The dark grey horizontal bars show 68% confidence intervals for A_{yr} predicted by S13, Kulier et al. (2013), labelled ‘K13’, Ravi et al. (2014), labelled ‘R14’, and McWilliams et al. (2014), labelled ‘M14’. The light grey shaded area indicates the 95% confidence PPTA upper limit on the GWB amplitude, set at $A_{\text{yr}} = 2.4 \times 10^{-15}$.

(ii) When we adopt the massive galaxy merger timescale from Kitzbichler & White (2008) with the associated mass- and redshift-dependence, rather than from numerical simulations of galaxy mergers (L08), we obtain $A_{\text{yr}} = 7.4 \times 10^{-16}$. This represents a decrease of 0.24 dex over the fiducial model.

(iii) When we introduce a redshift-dependent normalisation, α , of the $M_{\bullet} - M_{\text{bul}}$ relation with $K = 1$ such that the normalisation is a factor of three greater at $z = 2$, we obtain $A_{\text{yr}} = 1.8 \times 10^{-15}$. This is an increase of 0.14 dex over the fiducial model.

(iv) Finally, when we explore the effects of either reducing or increasing the fraction of early-type galaxies which are ellipticals by 50%, we obtain an associated variation in A_{yr} of 5% (0.02 dex).

The first three modifications are clearly significant, as compared to the fourth: we depict the resulting values of A_{yr} in the top panel of Figure 1. While the effects of modifications (i) and (iii) are comparable in magnitude, adopting the galaxy merger timescales of Kitzbichler & White (2008) makes a large difference to the prediction of A_{yr} . This is expected, because the Kitzbichler & White (2008) merger timescales are roughly a factor of three longer than those of L08. Indeed, modification (ii) results in a value of A_{yr} that is lower than the 2.5% percentile of the distributions of A_{yr} values given the three observational uncertainties considered so far.

As an illustration of the full range of possible values

of the GWB amplitude given the uncertainties considered in $\Gamma(M_{\bullet}, z)$, the GSMF and the $M_{\bullet} - M_{\text{bul}}$ relation combined with modifications (1) – (3) listed above, we generated a new sample of 600 realisations of A_{yr} . In this case, we simultaneously randomised over $\Gamma(M_{\bullet}, z)$, the GSMF and the $M_{\bullet} - M_{\text{bul}}$ relation as described above, and also (i) decreased the early-type GSMF by a factor uniformly drawn from the interval $[0, 1/3]$, (ii) set the galaxy merger timescale at a value uniformly drawn between the predictions of L08 and Kitzbichler & White (2008) (neglecting any mass- or redshift- dependence), and (iii) set the redshift-evolution index K of the normalisation of the $M_{\bullet} - M_{\text{bul}}$ relation to a number uniformly drawn from the interval $[0, 1]$. A histogram of the resulting sample of realisations of A_{yr} is shown in the bottom panel of Figure 1, labelled ‘All’. The long tail to lower values of A_{yr} , which is not reflected in the other histograms, is caused specifically by the inclusion of uncertainties in the galaxy merger timescale and in the early-type GSMF. The magnitudes of these effects on A_{yr} are indicated by the arrows at the top of Figure 1. The 95% confidence interval on A_{yr} , considering all uncertainties, is $5.1 \times 10^{-16} < A_{\text{yr}} < 2.4 \times 10^{-15}$.

We next compare our results for A_{yr} with earlier predictions. In Figure 2, we again show the histogram of realisations of A_{yr} corresponding to randomisation over all uncertainties, as well as the values of A_{yr} corresponding to modifications (i) to (iii) listed above. Above these, we show the 68% confidence intervals on A_{yr} from four recent, independent models for the binary SMBH population (S13; Kulier et al. 2013; Ravi et al. 2014; McWilliams et al. 2014). The predictions that we consider all account for the most recent determinations of the $M_{\bullet} - M_{\text{bul}}$ relation (Kormendy & Ho 2013; Scott et al. 2013).

The range of possible values of A_{yr} predicted by S13 is consistent with (albeit somewhat broader than) the range we predict given all uncertainties that we consider in this paper. Both the present work and S13 attempt to synthesise all uncertainties in quantities relevant to characterising the SMBH-SMBH coalescence rate, and use the same underlying model assumptions to predict the GWB amplitude. Our range of predictions is less extended than that of S13 because of the greater uncertainty assumed by S13 in the GSMF and the galaxy merger rate.¹

A semi-analytic approach (Guo et al. 2011) was used by Ravi et al. (2014) to predict SMBH-SMBH coalescence rates within the Millennium simulation (Springel et al. 2005), coupled with prescriptions for binary SMBH orbital evolution in stellar environments (Sesana 2010). The results of Ravi et al. (2014) indicate that the characteristic strain spectrum may be attenuated relative to the case of circular binary orbits and GW-driven evolution at frequencies $f \lesssim 10^{-8}$ Hz. However, the 68% confidence interval on the characteristic strain spectral amplitude at a frequency of f_{yr} is consistent with the range of values of A_{yr} we find.

¹ Some methodological differences also exist between the present work and S13 in how different realisations of A_{yr} were obtained.

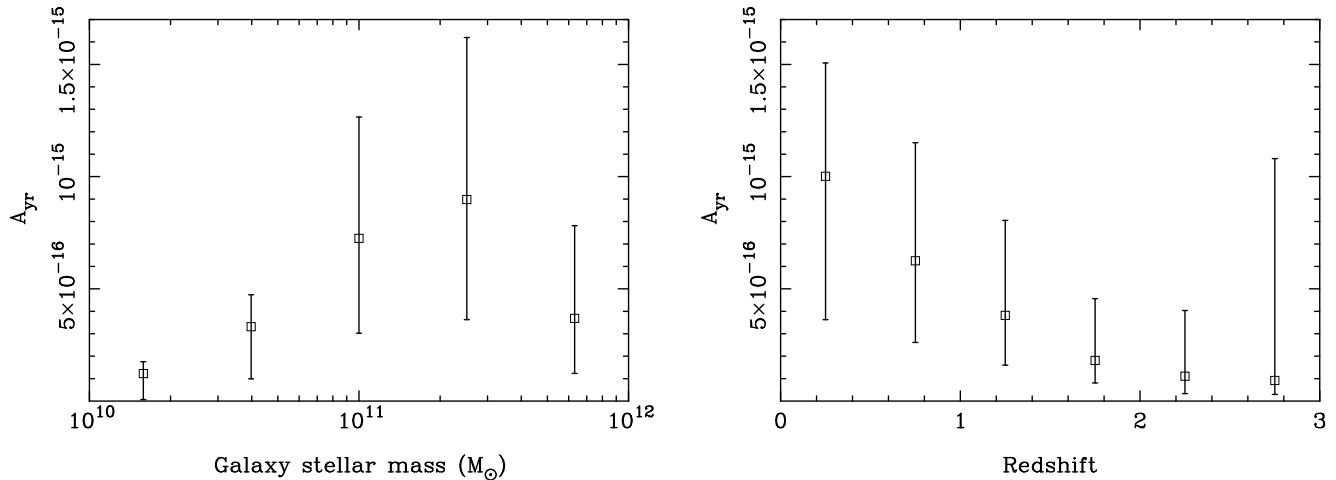


Figure 3. *Left:* Values of A_{yr} from binary SMBHs created in major mergers involving galaxies of different stellar masses. The squares indicate the fiducial model result, and the vertical error bars indicate 95% confidence intervals from 600 realisations of the model with all uncertainties that we account for. *Right:* Values of A_{yr} from binary SMBHs in six redshift bins in the interval $0 < z < 3$. The squares and error bars are as in the left panel. The redshift intervals correspond to the ranges within which the GSMF was evaluated by Muzzin et al. (2013).

The prediction of Kulier et al. (2013) is derived from hydrodynamic numerical galaxy formation simulations in cluster and field environments, but may be biased relative to semi-analytic galaxy formation models implemented in large-volume numerical dark matter simulations because of the specific choice of overdense and underdense regions to study. However, the prediction of Kulier et al. (2013) naturally includes a particularly sophisticated treatment of galaxy merger timescales.

McWilliams et al. (2014) suggest a model for the binary SMBH population which includes the assumption that all evolution in the early-type GSMF at $z < 1$ is driven by galaxy mergers; however, their predicted GWB amplitude appears to be inconsistent with current PTA constraints (Shannon et al. 2013). This model would necessarily include a shorter galaxy merger timescale than that predicted by L08 in order to maintain consistency with the observed numbers of merging galaxies. Overall, besides the study of McWilliams et al. (2014), it is encouraging that different models appear to agree on the amplitude of the characteristic strain spectrum from binary SMBHs. In particular, the upper ends of most predicted ranges of A_{yr} all appear to be consistent.

In Figure 2, we also depict the best existing 95% confidence upper limit on A_{yr} from Shannon et al. (2013) as a shaded region. Some realisations of A_{yr} given observational uncertainties in our model are inconsistent with this upper limit. However, the upper limit is generally consistent with our model given all uncertainties.

In Figure 3, we plot the values of A_{yr} predicted by the fiducial model in different ranges of M_* (left panel) and z (right panel). We also show the 95% confidence intervals on these values given all uncertainties we consider. The galaxy mass ranges correspond to the values of M_* of the larger galaxies in mergers. The dominant contributions to

the GWB are from binary SMBHs formed in mergers involving galaxies with $M_* \gtrsim 5 \times 10^{10} M_\odot$, and from binary SMBHs at redshifts $z \lesssim 1.5$. The confidence intervals that we provide further suggest that contributions to the GWB from outside these ranges are not significant.² Finally, binary SMBHs created in mergers involving at least one late-type galaxy correspond to $A_{\text{yr}} = 4.7 \times 10^{-16}$, whereas mergers involving only early-type galaxies correspond to $A_{\text{yr}} = 1.2 \times 10^{-15}$. Hence, within our model, the GWB is likely to be dominated by galaxy mergers involving only early-type galaxies (S0s and ellipticals).

3.2 Individual GW sources: continuous waves and memory bursts

In the process of evaluating Equation 15, we also calculated the numbers of individual binary SMBHs that produce monochromatic (CW) GW signals, along with the numbers of GW memory bursts emitted during SMBH-SMBH coalescence events. We counted individual binaries emitting GWs at frequencies $f = f_{\text{yr}}$ in a frequency bin of width $\Delta f = (10 \text{ yr})^{-1}$ and evaluated the numbers of binaries with different GW strain amplitudes h_s . These results are shown in the left panel of Figure 4 for the fiducial model as well as for two variations to the fiducial model (modifications (ii) and (iii) listed above). We also show results for the fiducial model while restricting the source counts to binaries at redshifts $z < 1$ and with the more massive progenitor galaxy

² While the most massive galaxies do not appear to contribute significantly to the GWB, it is apparent from, e.g., Figure 6 of Muzzin et al. (2013) (see also Baldry et al. 2012) that the Schechter function fits to the early-type GSMFs under-predict the observed GSMF at masses $M_* \gtrsim 10^{11.5}$.

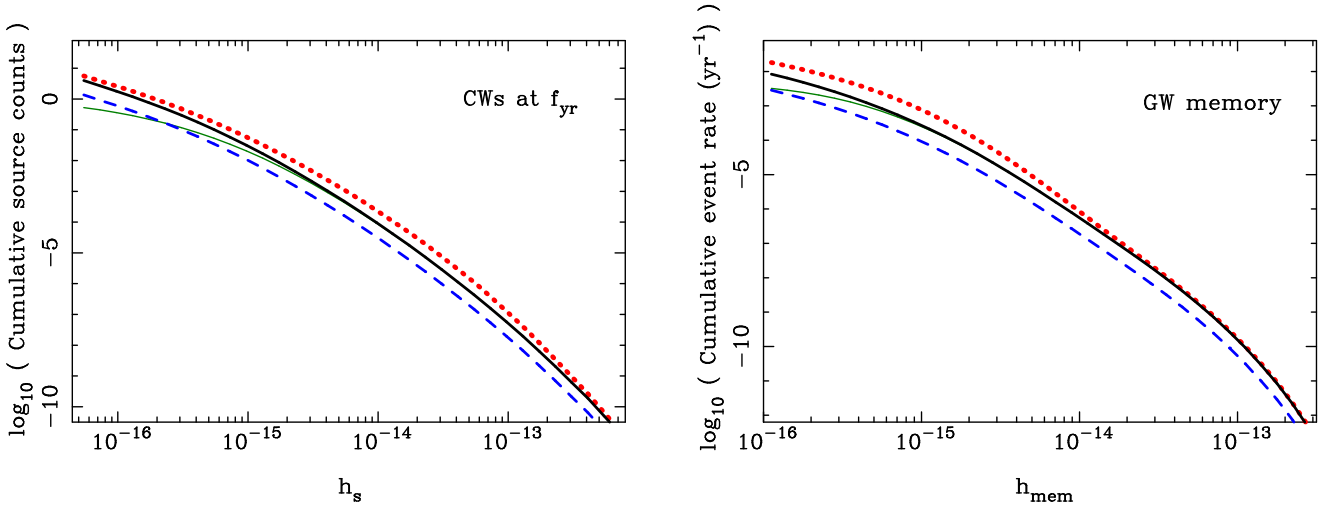


Figure 4. *Left:* the counts of individual sources at and above given GW strain amplitudes (h_s) at a GW frequency of f_{yr} in a frequency bin of width $\Delta f = (10 \text{ yr})^{-1}$. *Right:* the numbers of GW memory bursts per year at and above given strain amplitudes (h_{mem} , Equation 12). In both panels, the results of the fiducial model are shown as thick black solid curves, the results from a model with maximal redshift evolution in the $M_\bullet - M_{\text{bul}}$ relation ($K = 1$ corresponding to α in Equations 6 and refeq:c7e10 increased by a factor of three at $z = 2$) are shown as dotted red curves, and the results from a model with galaxy merger timescales consistent with Kitzbichler & White (2008) are shown as blue dashed curves. The green thin solid curves represent source counts for the fiducial model evaluated with the restrictions $z < 1$ and $M_* > 10^{11} M_\odot$.

mass $M_* > 10^{11} M_\odot$. The restricted source counts are identical to the full source counts for $h_s \gtrsim 2 \times 10^{-15}$. From Sesana et al. (2009), the characteristic amplitude of the sinusoidal ToA variations induced by a binary SMBH with strain amplitude h_s at $f = f_{yr}$, over a 10 yr observation, is $\sigma_R = 21(h_s/10^{-15}) \text{ ns}$.

Scaling these CW source counts to other GW frequencies is non-trivial. The GW strain amplitude of a binary SMBH radiating at a frequency f can be expressed as $h_s = h_{s, yr}(f/f_{yr})^{2/3}$, where $h_{s, yr}$ is the strain amplitude radiated by that binary at a frequency f_{yr} . Furthermore, the total number of binaries per unit frequency radiating GWs at a frequency f is related to the number of binaries per unit frequency radiating GWs at f_{yr} by the factor $(f/f_{yr})^{-11/3}$, assuming GW-driven binary orbital evolution. Then, the number of binaries per unit frequency emitting GWs at or above a strain amplitude of h_s , at a frequency f , may be written as $n(f, h_s) = n(f_{yr}, h_s(f/f_{yr})^{-2/3})(f/f_{yr})^{-11/3}$. For example, while the fiducial model predicts $\sim 10^{-2}$ CW sources with $h_s \geq 10^{-15}$ in a frequency bin of width $\Delta f = (10 \text{ yr})^{-1}$ at $f = f_{yr}$, this prediction changes to ~ 0.1 sources at $f = f_{yr}/5$ with $h_s \geq 10^{-15}$ in the same frequency bin width.

We can hence directly compare our predicted CW source counts with the work of Sesana et al. (2009). These authors considered a wide variety of SMBH growth scenarios within the framework of a semi-analytic model for galaxy formation (Bertone et al. 2007) implemented in the Millennium simulation results (Springel et al. 2005). We directly compare predictions for the number of binary SMBHs inducing ToA variations with characteristic amplitudes $\sigma_R \geq 30 \text{ ns}$. For consistency, we consider an observation time span of $T = 5 \text{ yr}$ and GW frequencies $f > 3 \times 10^{-9} \text{ Hz}$, and in-

tegrate over the number of sources per unit frequency with $\sigma_R \geq 30 \text{ ns}$ in the range $3 \times 10^{-9} - 10^{-7} \text{ Hz}$ (integrating to higher frequencies does not significantly alter our results). We neglect the issue of whether these signals are resolvable given the presence of a GWB. We predict 0.6 CW sources with $\sigma_R \geq 30 \text{ ns}$ for our fiducial model, 0.1 CW sources for a pessimistic model assuming the galaxy merger timescales of Kitzbichler & White (2008), and 1.2 CW sources for our optimistic model with significant redshift-evolution in the $M_\bullet - M_{\text{bul}}$ relation. Sesana et al. (2009) predict between 0.05 and 3 such sources (their Figure 3), which is consistent with our results.

We also predicted the numbers of binary SMBH coalescence events per observed year at or above a given GW memory burst amplitude, h_{mem} (see Equation 12) for $h_{\text{mem}} > 10^{-16}$. The results are shown in the right panel of Figure 4, again for the fiducial model and two variations to this model. We also again show results for the fiducial model with the restrictions of $z < 1$ and $M_* > 10^{11} M_\odot$; for $h_{\text{mem}} \gtrsim 6 \times 10^{-16}$, the restrictions make no significant difference.

In summary, the expected numbers of individual GW sources predicted by our empirical binary SMBH model are small. At most ~ 1 CW source is expected to induce ToA variations with characteristic amplitudes $\geq 30 \text{ ns}$ over a 5 yr observation time span. Also, approximately one GW memory burst with $h_{\text{mem}} > 5 \times 10^{-16}$ is expected every 1000 yr.

4 IMPLICATIONS FOR GW DETECTION WITH PTAS

4.1 The GWB from binary SMBHs

The future sensitivities of PTAs to the GWB are the subjects of ongoing research (e.g., Siemens et al. 2013; Moore et al. 2014; Hobbs et al. 2014). For example, future pulsar observing systems and cadences, new pulsar discoveries, the effects of the interstellar medium and pulsar timing noise characteristics, all of which significantly affect PTA sensitivities, are difficult to forecast because of a lack of quantitative, predictive models. An idealised treatment of the problem by Siemens et al. (2013) suggests that, for the NANOGrav collaboration, a GWB with amplitude $A_{\text{yr}} = 10^{-15}$ may be detectable before the year 2020. We note that Siemens et al. (2013) assumed that the GWB characteristic strain spectrum has the power law form given in Equation 1. We find in this paper that the GWB amplitude is likely to be in the range $5.1 \times 10^{-16} < A_{\text{yr}} < 2.4 \times 10^{-15}$ with 95% confidence. If the GWB amplitude were to lie in the upper part of this range, as is expected given the more commonly preferred major galaxy merger timescale (L08), we suggest that detecting a GWB from binary SMBHs is indeed an attainable, short-term goal for PTAs.³

What can PTA upper limits on or detections of the GWB reveal about the determinants of the GWB amplitude? The GWB may be parameterised by a single number, A_{yr} (at least at GW frequencies $f \gtrsim 10^{-8}$ Hz; Ravi et al. 2014), the value of which is dependent on myriad quantities. Useful information can be gleaned if one of these quantities is particularly unconstrained otherwise. For example, if we remain agnostic with respect to the galaxy merger timescale, a particular value of this timescale would correspond to a range of possible GWB amplitudes given our knowledge of all the other determinants of A_{yr} . Then, a PTA constraint on A_{yr} would correspond to a constraint on the galaxy merger timescale, given the assumptions inherent in our model. Through such exercises, PTAs could directly impact our understanding of galaxy and SMBH growth, in a more general sense than by testing specific GWB models using PTA data. We leave a demonstration of such techniques for future work.

4.2 CW signals from individual binary SMBHs

Future PTA observations with planned telescopes such as the Five Hundred Metre Aperture Spherical Telescope (FAST, Li, Nan & Pan 2013) and the Square Kilometre Array (SKA, Cordes et al. 2004) may include up to 100 pulsars with timing noise standard deviations of ~ 100 ns (Lazio 2013; Hobbs et al. 2014). Ellis et al. (2012) constructed theoretical PTA sensitivity curves using simulated data sets with both 100 arbitrarily-located pulsars or 17 pulsars at

the locations of the best-timed pulsars observed by the NANOGrav collaboration, in all cases with timing noise standard deviations of 100 ns and 5 yr observation times. These sensitivity curves, shown in their Figure 5, represent the values of h_s at different frequencies at which the probability of a false detection was less than 10^{-4} in 95% of realisations of their simulated data sets. Importantly, the sensitivity curves were averaged over all source positions and orientations, and account for pulsar parameter fitting. We predict the numbers of detectable sources for PTAs with these sensitivity curves by evaluating the following integral:

$$N_{\text{detect}} = \int_{(10 \text{ yr})^{-1}}^{10^{-7} \text{ Hz}} \frac{dF[h_{\text{sens}}(f)]}{df} df, \quad (16)$$

where $h_{\text{sens}}(f)$ is the sensitivity curve and $\frac{dF(h_{\text{sens}})}{df}$ is the predicted number of sources with strain amplitudes $h_s \geq h_{\text{sens}}(f)$ per unit frequency at a frequency f . The sensitivities of PTAs to CW sources are generally poor for frequencies $f \gtrsim 10^{-7}$ Hz and few sources are expected at these frequencies.

Using our predictions for the numbers of CW sources, we evaluate $\frac{dF(h_{\text{sens}})}{df}$ by scaling the predictions as described in §3.2. Then, for the fiducial model and for the two sensitivity curves of Ellis et al. (2012) corresponding to their coherent \mathcal{F} -statistic, we obtain predictions of 0.07 and 1.3 detectable sources for the 17- and 100-pulsar cases respectively. For the restricted fiducial model, corresponding only to sources with $z < 1$ and $M_* > 10^{11} M_{\odot}$ these reduce marginally to 0.06 and 1 source respectively. For the optimistic case with strong redshift-evolution of the $M_{\bullet} - M_{\text{bul}}$ relation, we obtain predictions of 0.2 and 2.8 detectable sources for the 17- and 100-pulsar cases respectively. In contrast, the current PPTA sensitivity curve produced by Zhu et al. (2014) corresponds to $\lesssim 10^{-4}$ detectable sources. ‘Noise’ caused by the summed GW signal from the binary SMBH population will further increase the difficulty of detecting individual binaries (e.g., Sesana et al. 2009; Ravi et al. 2012).

4.3 GW memory bursts from coalescing binary SMBHs

A PTA data set with 20 pulsars timed with a precision of 100 ns for 10 yr is sensitive to memory bursts with amplitudes $h_{\text{mem}} > 5 \times 10^{-15}$ over 70 – 80% of the data span (van Haasteren & Levin 2010; Cordes & Jenet 2012). As the sensitivity of such an idealised PTA to memory bursts scales roughly as the square root of the number of pulsars (van Haasteren & Levin 2010), a PTA with 100 pulsars timed with 100 ns precision for 10 yr may be sensitive to memory bursts with $h_{\text{mem}} > 2 \times 10^{-15}$. However, our model suggests that only $\sim 10^{-5}$ bursts with $h_{\text{mem}} > 5 \times 10^{-15}$ and $\sim 10^{-3}$ bursts with $h_{\text{mem}} > 2 \times 10^{-15}$ are expected over 10 yr. Thus, under the model presented here, GW memory bursts from coalescing binary SMBHs do not represent viable sources for PTAs.

³ If we calculate the range of possible A_{yr} values given all uncertainties, while assuming the L08 galaxy merger timescales, we find $A_{\text{yr}} > 9 \times 10^{-16}$ with 95% confidence.

5 DISCUSSION

Our predictions for the GWB amplitude, A_{yr} , are conservative within their respective scenarios, for a number of reasons. (i) We do not account for minor galaxy mergers with stellar mass ratios $\mu_* < 1/3$, or for mergers where the more massive galaxy has a mass $M_* < 10^{10} M_\odot$. (ii) We do not consider the possibility of gas accretion onto SMBHs prior to coalescence during galaxy mergers (e.g., Van Wassenhove et al. 2012), which would raise the SMBH masses and hence the emitted GW amplitudes (e.g., Sesana et al. 2008). (iii) The most massive galaxies are typically found in cluster environments, where times between galaxy mergers may be shorter (cf. Lotz et al. 2013), implying a higher merger rate for these galaxies and hence a higher GW signal. However, we do not expect the inclusion of these factors to significantly affect our predicted GWB amplitudes. We reiterate that the effects of interactions between binary SMBHs and their environments are unlikely to affect the predictions for the GWB amplitude at frequencies $f \gtrsim 10^{-8}$ Hz (Sesana 2013b; Ravi et al. 2014), such as at f_{yr} . This is because the orbital evolution of binary SMBHs radiating GWs at these frequencies is expected to be predominantly GW-driven, which further leads to the circularisation of the orbits.

Of all sources of uncertainty we consider in predicting the GWB amplitude given relevant observational quantities, the choice of galaxy merger timescale dominates the range of possible GWB amplitudes. Furthermore, the merger timescale may be even more uncertain than the range spanned by the predictions we consider (L08; Kitzbichler & White 2008). The simulations of L08 were conducted only for mergers between gas-rich disk galaxies, some of which contained small bulges, whereas we find that the GWB is likely dominated by binary SMBHs formed in mergers solely between early-type galaxies. Further theoretical studies of galaxy merger timescales for early-type systems are clearly required in order to better predict the GWB amplitude. The dominance of low-redshift ($z \lesssim 1.5$) early-type major galaxy mergers of massive ($M_* \gtrsim 5 \times 10^{10} M_\odot$) galaxies in determining the GWB amplitude is a further important consequence of our work for both theoretical and observational studies of galaxy mergers aimed at informing PTA research.

The other significant source of uncertainty in our predictions is in the $M_\bullet - M_{\text{bul}}$ relation, both in its local form and in its possible redshift-evolution. In contrast to uncertainty in the galaxy merger timescale, it is likely that this uncertainty will only be resolved through further observations which significantly expand the sample of known SMBH masses. Promisingly, Davis et al. (2013) report that hundreds of SMBH mass measurements may be possible with the Atacama Large Millimetre Array (ALMA).

Under what circumstances could the GWB amplitude lie outside the range we predict given all uncertainties that we consider? The predicted range of GWB amplitudes, $5.1 \times 10^{-16} < A_{\text{yr}} < 2.4 \times 10^{-15}$, encompasses all purely observational uncertainties, as well as uncertainty ranges

that we set for other quantities for which observational constraints are poor, such as the galaxy merger timescale. It may be possible that these latter ranges are incorrect. Furthermore, not all galaxies may host a central SMBH, as we have assumed. The interaction between a binary SMBH and a third SMBH would likely cause the least massive SMBH to be ejected (e.g., Gerosa & Sesana 2014), lowering the number of coalescing SMBHs. If not every massive galaxy at $z \sim 1$ formed with a central SMBH, the GWB amplitude would again be lowered. It may also be possible that binary SMBHs do not always coalesce on timescales less than the times between galaxy mergers.

The presence of a few strong GW emitters among the binary SMBH population implies that some excess, non-Gaussian scatter will be present in the GW signals produced by this population. The magnitude of this excess scatter in A_{yr} depends on exactly how many binary SMBH systems contribute significantly to the GWB. Using a semi-analytic galaxy formation model implemented in the Millennium simulation (Guo et al. 2011), Ravi et al. (2012) suggested that the statistics of ToA variations induced by GWs from binary SMBHs are mildly non-Gaussian for frequencies $f > f_{\text{yr}}/5$ because of appreciable contributions to the squared characteristic strain spectrum, $h_c^2(f)$, from individual binaries at every GW frequency. Figure 5 shows the number of binary SMBHs in our fiducial model corresponding to galaxy mergers with primary stellar masses greater than or equal to a given M_* (top), as well as the fractions of A_{yr}^2 contributed by these binaries (bottom). We show in particular binaries radiating at a GW frequency of f_{yr} in a frequency bin of width $\Delta f = (10 \text{ yr})^{-1}$. Our fiducial model suggests that the contributions of individual GW sources to $h_c^2(f)$ are lower than estimated by Ravi et al. (2012). For example, the modelling in Ravi et al. (2012) found that one source contributed $\sim 50\%$ of $h_c^2(f)$ at a frequency of $2f_{\text{yr}}/3$ in a frequency bin of width $(5 \text{ yr})^{-1}$ (their Figure 2). In contrast, our empirical modelling in this paper suggests that the strongest ~ 400 sources in such a frequency bin contribute $\sim 50\%$ of $h_c^2(2f_{\text{yr}}/3)$.

This work and Ravi et al. (2012) clearly predict different numbers of the most massive binary SMBHs. While this discrepancy will only be resolved with GW observations, we point out that the Schechter functions for the GSMFs that we use under-predict observed galaxy counts at the highest masses and the lowest redshifts (Baldry et al. 2012; Muzzin et al. 2013). Hence, it is possible that our model under-represents the contributions of the most massive binary SMBHs to the total GW signal. Differing typical galaxy merger mass ratios in cluster and field environments (e.g., Lotz et al. 2013) are a further complicating factor.

6 CONCLUSIONS

In this paper, we predicted the strength of the GWB from binary SMBHs and the occurrence of individual binary SMBH GW sources. Our approach was to use a selection of recent observational estimates for the average times between major

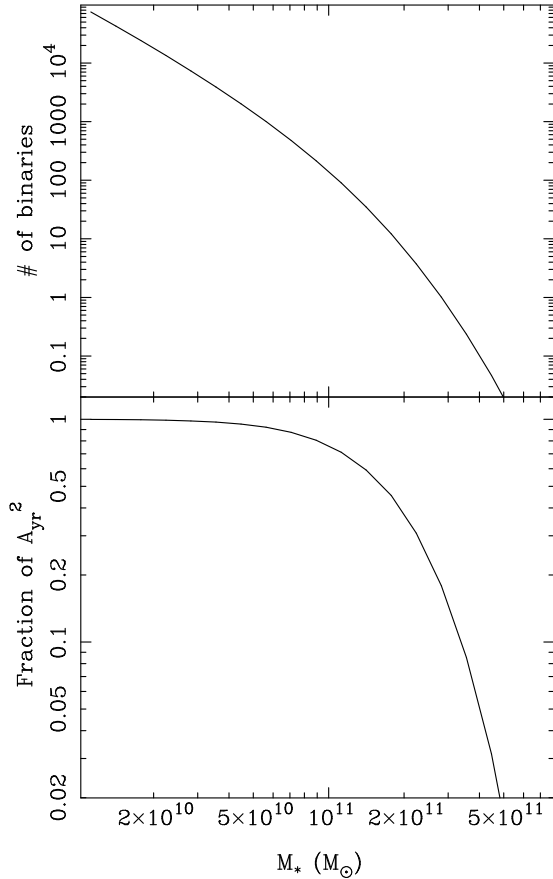


Figure 5. *Top:* The numbers of binary SMBH sources predicted by our fiducial model radiating at a GW frequency of f_{yr} in a frequency bin of width $\Delta f = (10 \text{ yr})^{-1}$ at and above given values of M_* . *Bottom:* The fractions of A_{yr}^2 contributed by binary SMBHs at and above given values of M_* .

mergers for galaxies with $M_* > 10^{10} M_\odot$ and $z < 3$ and for the GSMFs of early- and late-type galaxies in this mass and redshift range. We combined these quantities with empirical relations between galaxy and bulge stellar masses and between bulge and SMBH masses.

We find that while current PTAs are unlikely to be sensitive to individual binary SMBHs, a PTA consisting of ~ 100 pulsars timed with ~ 100 ns precision for 5 yr will be sensitive to up to ~ 3 binary SMBHs. Such a PTA may be achievable with the SKA (Lazio 2013), but is possibly beyond the capabilities of FAST (Hobbs et al. 2014). Even such a PTA will, however, have a less than 0.1% chance of detecting a GW memory burst from a coalescing binary SMBH. Thus, we conclude that while individual binary SMBHs may be detectable with a PTA based on next-generation radio telescopes, memory bursts from coalescing SMBHs are not likely to be detectable with any envisaged PTA.

We predict that the characteristic strain amplitude of the GWB lies in the range $5.1 \times 10^{-16} < A_{\text{yr}} < 2.4 \times 10^{-15}$ with 95% confidence, accounting for a variety of uncertainties. The upper end of the predicted amplitude range is

equivalent to the best published 95% confidence upper limit on the GWB amplitude (Shannon et al. 2013). This reinforces the conclusion of Shannon et al. (2013) that some models for the binary SMBH population that are consistent with current electromagnetic observations are already inconsistent with PTA constraints on the GWB.

The dominant uncertainty in predicting the GWB amplitude appears to be caused by differences in theoretical predictions for the major merger timescale of massive galaxies. Higher values within our predicted range for A_{yr} correspond to the more commonly preferred choice of galaxy merger timescale (L08); GWB amplitudes $A_{\text{yr}} > 10^{-15}$ are within the sensitivity ranges of current and future PTAs. We strongly urge further work on quantifying the galaxy merger timescale, in particular for the mergers between massive early-type galaxies at redshifts $z < 1.5$ which are likely to host the dominant contributors to the GWB. The other significant uncertainty in our predictions is in the local form and possible redshift-evolution of the $M_\bullet - M_{\text{bul}}$ relation. PTA upper limits on or detections of the GWB may be able to meaningfully improve our knowledge of such otherwise poorly constrained facets of the formation and evolution of galaxies and SMBHs.

ACKNOWLEDGEMENTS

The authors thank Alberto Sesana for useful discussions and Justin Ellis for sharing results on predicted sensitivity curves. The authors also acknowledge the comments of the anonymous referee, which helped to significantly improve the manuscript. V.R. is a recipient of a John Stocker Postgraduate Scholarship from the Science and Industry Endowment Fund and J.S.B.W. acknowledges an Australian Research Council Laureate Fellowship. GH is supported by an Australian Research Council Future Fellowship. This work was performed on the swinSTAR supercomputer at the Swinburne University of Technology.

REFERENCES

- Aller, M. C., & Richstone, D. 2002, *AJ*, 124, 3035
- Arzoumanian, Z., Brazier, A., Burke-Spolaor, S., et al. 2014, arXiv:1404.1267
- Baldry I. K., Driver S. P., Loveday J., Taylor E. N., Kelvin L. S., Liske J., Norberg P., Robotham A. S. G., Brough S., Hopkins A. M., Bamford S. P. et al., 2012, *MNRAS*, 421, 621
- Barnes J. E., Hernquist L., 1992, *ARA&A*, 30, 705
- Begelman M. C., Blandford R. D., Rees M. J., 1980, *Nat*, 287, 307
- Bernardi, M., Shankar, F., Hyde, J. B., et al. 2010, *MNRAS*, 404, 2087
- Bertone, S., De Lucia, G., & Thomas, P. A. 2007, *MNRAS*, 379, 1143
- Borison T. A., Lauer T. R., 2009, *Nat*, 458, 53
- Braginskii V. B., Thorne K. S., 1987, *Nat*, 327, 123

- Bundy, K., Fukugita, M., Ellis, R. S., et al. 2009, *ApJ*, 697, 1369
- Conselice C. J., 2003, *ApJS*, 147, 1
- Conselice, C. J. 2014, arXiv:1403.2783
- Conselice C. J., Yang C., Bluck A. F. L., 2009, *MNRAS*, 394, 1956
- Cordes, J. M., & Shannon, R. M. 2010, arXiv:1010.3785
- Cordes J. M., Jenet F. A., 2012, *ApJ*, 752, 54
- Cordes J. M., Kramer M., Lazio T. J. W., Stappers B. W., Backer D. C., Johnston S., 2004, *New Astronomy Review*, 48, 1413
- Courteau, S., Cappellari, M., de Jong, R. S., et al. 2014, *Reviews of Modern Physics*, 86, 47
- Davis, T. A., Bureau, M., Cappellari, M., Sarzi, M., & Blitz, L. 2013, *Nature*, 494, 328
- de Ravel, L., Le Fèvre, O., Tresse, L., et al. 2009, *A&A*, 498, 379
- Detweiler S., 1979, *ApJ*, 234, 1100
- Dotti, M., Colpi, M., Haardt, F., & Mayer, L. 2007, *MNRAS*, 379, 956
- Ellis J. A., Siemens X., Creighton J. D. E., 2012, *ApJ*, 756, 175
- Emsellem, E., Cappellari, M., Krajnović, D., et al. 2011, *MNRAS*, 414, 888
- Enoki M., Inoue K. T., Nagashima M., Sugiyama N., 2004, *ApJ*, 615, 19
- Eracleous, M., Boroson, T. A., Halpern, J. P., & Liu, J. 2012, *ApJS*, 201, 23
- Escala A., Larson R. B., Coppi P. S., Mardones D., 2004, *ApJ*, 607, 765
- Estabrook F. B., Wahlquist H. D., 1975, *General Relativity and Gravitation*, 6, 439
- Favata M., 2009, *ApJ*, 696, L159
- Foster R. S., Backer D. C., 1990, *ApJ*, 361, 300
- Frank J., Rees M. J., 1976, *MNRAS*, 176, 633
- Gerosa, D., & Sesana, A. 2014, arXiv:1405.2072
- Graham, A. W., Onken, C. A., Athanassoula, E., & Combes, F. 2011, *MNRAS*, 412, 2211
- Guo Q., White S., Boylan-Kolchin M., De Lucia G., Kauffmann G., Lemson G., Li C., Springel V., Weinmann S., 2011, *MNRAS*, 413, 101
- Hellings, R. W., & Downs, G. S. 1983, *ApJL*, 265, L39
- Hobbs G., Jenet F., Lee K. J., Verbiest J. P. W., Yardley D., Manchester R., Lommen A., Coles W., Edwards R., Shettigara C., 2009, *MNRAS*, 394, 1945
- Hobbs, G., Archibald, A., Arzoumanian, Z., et al. 2010, *Classical and Quantum Gravity*, 27, 084013
- Hobbs, G., Dai, S., Manchester, R. N., et al. 2014, arXiv:1407.0435
- Hopkins, P. F., Croton, D., Bundy, K., et al. 2010, *ApJ*, 724, 915
- Jaffe A. H., Backer D. C., 2003, *ApJ*, 583, 616
- Jiang, C. Y., Jing, Y. P., Faltenbacher, A., Lin, W. P., & Li, C. 2008, *ApJ*, 675, 1095
- Khan F. M., Preto M., Berczik P., Berentzen I., Just A., Spurzem R., 2012, *ApJ*, 749, 147
- Kitzbichler, M. G., & White, S. D. M. 2008, *MNRAS*, 391, 1489
- Kormendy J., Ho L. C., 2013, *ARA&A*, 51, 511
- Kramer, M., & Champion, D. J. 2013, *Classical and Quantum Gravity*, 30, 224009
- Kulier, A., Ostriker, J. P., Natarajan, P., Lackner, C. N., & Cen, R. 2013, arXiv:1307.3684
- Lackner, C. N., & Gunn, J. E. 2012, *MNRAS*, 421, 2277
- Lazio, T. J. W. 2013, *Classical and Quantum Gravity*, 30, 224011
- Lee, K. J., Wex, N., Kramer, M., et al. 2011, *MNRAS*, 414, 3251
- Li D., Nan R., Pan Z., 2013, in *IAU Symposium Vol. 291 of IAU Symposium, The Five-hundred-meter Aperture Spherical radio Telescope project and its early science opportunities*, pp 325–330
- López-Sanjuan, C., Le Fèvre, O., Ilbert, O., et al. 2012, *A&A*, 548, A7
- Lotz J. M., Jonsson P., Cox T. J., Primack J. R., 2008, *MNRAS*, 391, 1137
- Lotz, J. M., Jonsson, P., Cox, T. J., & Primack, J. R. 2010, *MNRAS*, 404, 575
- Lotz J. M., Papovich C., Faber S. M., Ferguson H. C., Grogan N., Guo Y., Kocevski D., Koekemoer A. M., Lee K.-S., McIntosh D., Momcheva I., Rudnick G., Saintonge A., Tran K.-V., van der Wel A., Willmer C., 2013, *ApJ*, 773, 154
- Madison, D. R., Cordes, J. M., & Chatterjee, S. 2014, arXiv:1404.5682
- Manchester R. N., Hobbs G., Bailes M., Coles W. A., van Straten W., Keith M. J., Shannon R. M., Bhat N. D. R., Brown A., Burke-Spolaor S. G., Champion D. J., et al. 2013, *PASA*, 30, 17
- Manchester R. N., IPTA 2013, *Classical and Quantum Gravity*, 30, 224010
- McLaughlin, M. A. 2013, *Classical and Quantum Gravity*, 30, 224008
- McWilliams, S. T., Ostriker, J. P., & Pretorius, F. 2014, *ApJ*, 789, 156
- Meert, A., Vikram, V., & Bernardi, M. 2014, arXiv:1406.4179
- Mendel, J. T., Simard, L., Palmer, M., Ellison, S. L., & Patton, D. R. 2014, *ApJS*, 210, 3
- Merritt D., Milosavljević M., 2005, *Living Reviews in Relativity*, 8, 8
- Miller, B. P., Gallo, E., Greene, J. E., et al. 2014, arXiv:1403.4246
- Mitchell, P. D., Lacey, C. G., Baugh, C. M., & Cole, S. 2013, *MNRAS*, 435, 87
- Moore, C. J., Taylor, S. R., & Gair, J. R. 2014, arXiv:1406.5199
- Muzzin A., Marchesini D., Stefanon M., Franx M., McCracken H. J., Milvang-Jensen B., Dunlop J. S., Fynbo J. P. U., Brammer G., Labbé I., van Dokkum P. G., 2013, *ApJ*, 777, 18
- Peters P. C., Mathews J., 1963, *Physical Review*, 131, 435
- Phinney, E. S. 2001, arXiv:astro-ph/0108028
- Planck Collaboration, Ade, P. A. R., Aghanim, N., et al. 2013, arXiv:1303.5076
- Quinlan G. D., 1996, *New Astronomy*, 1, 35

- Ravi V., Wyithe J. S. B., Hobbs G., Shannon R. M., Manchester R. N., Yardley D. R. B., Keith M. J., 2012, *ApJ*, 761, 84
- Ravi, V., Wyithe, J. S. B., Shannon, R. M., Hobbs, G., & Manchester, R. N. 2014, *MNRAS*, 442, 56
- Robotham, A. S. G., Driver, S. P., Davies, L. J. M., et al. 2014, *arXiv:1408.1476*
- Rodriguez C., Taylor G. B., Zavala R. T., Peck A. B., Pollack L. K., Romani R. W., 2006, *ApJ*, 646, 49
- Roedig C., Dotti M., Sesana A., Cuadra J., Colpi M., 2011, *MNRAS*, 415, 3033
- Roedig, C., & Sesana, A. 2012, *Journal of Physics Conference Series*, 363, 012035
- Sazhin M. V., 1978, *SvA*, 22, 36
- Scott, N., Graham, A. W., & Schombert, J. 2013, *ApJ*, 768, 76
- Sesana A., 2010, *ApJ*, 719, 851
- Sesana A., 2013, *MNRAS*, 433, L1
- Sesana, A. 2013b, *Classical and Quantum Gravity*, 30, 224014
- Sesana, A., Haardt, F., Madau, P., & Volonteri, M. 2004, *ApJ*, 611, 623
- Sesana A., Vecchio A., Colacino C. N., 2008, *MNRAS*, 390, 192
- Sesana A., Vecchio A., Volonteri M., 2009, *MNRAS*, 394, 2255
- Shankar F., Weinberg D. H., Miralda-Escudé J., 2013, *MNRAS*, 428, 421
- Shannon R. M., Ravi V., Coles W. A., Hobbs G., Keith M. J., Manchester R. N., Wyithe J. S. B., Bailes M., Bhat N. D. R., Burke-Spolaor S., Khoo J., Levin Y., Oslowski S., Sarkissian J. M., van Straten W., Verbiest J. P. W., Want J.-B., 2013, *Science*, 342, 334
- Siemens X., Ellis J., Jenet F., Romano J. D., 2013, *Classical and Quantum Gravity*, 30, 224015
- Simard, L., Mendel, J. T., Patton, D. R., Ellison, S. L., & McConnell, A. W. 2011, *ApJS*, 196, 11
- Springel, V., White, S. D. M., Jenkins, A., et al. 2005, *Nat*, 435, 629
- Valtonen M. J., Lehto H. J., Nilsson K., Heidt J., Takalo L. O., Sillanpää A., Villforth C., Kidger M., Poyner G., Pursimo T., Zola S., Wu J.-H., Zhou X. e. a., 2008, *Nat*, 452, 851
- van Haasteren R., Levin Y., 2010, *MNRAS*, 401, 2372
- Van Wassenhove, S., Volonteri, M., Mayer, L., et al. 2012, *ApJL*, 748, L7
- Wyithe J. S. B., Loeb A., 2003, *ApJ*, 590, 691
- Xu C. K., Zhao Y., Scoville N., Capak P., Drory N., Gao Y., 2012, *ApJ*, 747, 85
- Yardley D. R. B., Hobbs G. B., Jenet F. A., Verbiest J. P. W., Wen Z. L., Manchester R. N., Coles W. A., van Straten W., Bailes M., Bhat N. D. R., Burke-Spolaor S., Champion D. J., Hotan A. W., Sarkissian J. M., 2010, *MNRAS*, 407, 669
- Yu Q., 2002, *MNRAS*, 331, 935
- Yu Q., Tremaine S., 2002, *MNRAS*, 335, 965
- Zhu, X.-J., Hobbs, G., Wen, L., et al. 2014, *arXiv:1408.5129*